DOI: 10.15669/pnst.7.273

Progress in Nuclear Science and Technology
Volume 7 (2025) pp. 273-278

ARTICLE

Effect of electrolyte particle size on CO_2 electrolysis performance of metal-supported solid oxide electrolysis cells prepared by atmospheric plasma spraying method

Kosuke Umeda [a], Yuko Maruyama [a], Sho Kuzukami [a], Shuzo Tominaga [a], Yukitaka Kato [b] and Hiroki Takasu [b,*]

[a] Graduate Major in Nuclear Engineering, Department of Chemical Science and Engineering, School of Materials and Chemical Technology, Institute of Science Tokyo, N1-22, 2-12-1 Ookayama, Meguro-ku, Tokyo 152-8550, Japan; [b] Laboratory for Zero-Carbon Energy, Institute of Integrated Research, Institute of Science Tokyo, N1-22, 2-12-1 Ookayama, Meguro-ku, Tokyo 152-8550, Japan

Reducing CO_2 emissions in the industrial sector is a neccessary task for the realization of a low-carbon society. In particular, for ironmaking processes with high CO_2 emissions, a system based on an active carbon recycling energy system (iACRES) has been proposed to reduce and recycle emitted CO_2. To establish iACRES, we studied CO_2 reduction technology using solid oxide electrolysis cells (SOECs). SOEC technology can efficiently convert CO_2 at high temperatures. However, ceramic-supported SOECs lack mechanical strength for large cell areas. To solve this problem, we developed a metal-supported SOEC (MS-SOEC). In this study, we performed CO_2 electrolysis using the new MS-SOEC, and evaluated the effect of electrolyte densification on electrolytic performance. The CO production rate of the cell with the densified electrolyte was 0.635 μmol s^{-1} cm^{-2} at 4 V and the total resistance was 16.8 Ω cm^{-2}. We anticipate that the improved performance of the developed cell will contribute to the construction of a low-carbon society.

Keywords: SOEC; CO_2 reduction; carbon recycling; MS-SOEC

1. Introduction

Since the industrial revolution of the late 18th century, the concentration of carbon dioxide (CO_2), a greenhouse gas, has continued to rise from approximately 280 ppm in 1850 to over 400 ppm today [1]. In response to this situation, the 21st Conference of the Parties (COP21) to the United Nations Framework Convention on Climate Change adopted an agreement to pursue efforts to limit the global temperature increase to 1.5°C from the pre-industrial revolution [2]. Realization of this goal will require worldwide reduction in CO_2 emissions. The Japanese government has declared its aim to achieve carbon neutrality by 2050 [3]. In its efforts to reduce CO_2 emissions, Japan has set stepwise CO_2 reduction targets of 46% and 100% for 2030 and 2050, respectively. Further reductions are likely required to meet this goal.

One measure that has been proposed is the active carbon recycling energy system (ACRES) [4]. ACRES uses non-fossil primary energy to recycle and reuse CO_2 as a carbon resource. This system enables carbon to be recycled and reused, providing energy without emitting CO_2 into the atmosphere. ACRES is expected to be applied industrially in the ironmaking process (smart ironmaking process based on ACRES or iACRES). CO_2 emissions from the steel industry account for approximately 15% of the total carbon emissions generated by the Japanese industrial sector [5]. Emissions from the ironmaking process account for approximately 70% of the total amount [6]. Therefore, applying this energy system to the ironmaking process is beneficial to realize low-carbon emissions. The CO_2 reduction process is a recycling flow in which carbon monoxide (CO) is generated from CO_2 emitted through the iron oxide reduction reaction and reused as a reductant. This reduces both coke consumption and CO_2 emissions in the ironmaking process. Therefore, iACRES is expected to contribute to the establishment of a new low-carbon ironmaking process through carbon cycling [7].

To establish iACRES, we studied CO_2 reduction technology using solid oxide electrolysis cells (SOECs). SOEC is an efficient high-temperature CO_2 electrolysis accomplished by applying a reverse potential to the cells of a solid oxide fuel cell (SOFC) structure [8-10]. In addition, from the Gibbs free energy equation ($\Delta G = \Delta H - T\Delta S$), additional thermal energy input reduces the electrical energy required to reduce CO_2 to CO. ΔG (change in Gibbs free energy), which is the electrical energy required for CO_2 electrolysis, is reduced by increasing the operating temperature. $T\Delta S$ (T: temperature, ΔS: change in entropy) represents the heat demand of the process [11].

---

*Corresponding author. E-mail: takasu.h.aa@m.titech.ac.jp

$$\mathrm{CO_2} \rightarrow \mathrm{CO} + 1/2\mathrm{O_2},\ \Delta H^\circ = 283\ \mathrm{kJ\ mol^{-1}} \quad \left(\Delta H^\circ : \text{change in standard enthalpy}\right) \tag{1}$$

An SOEC consists of a cathode, anode, and solid electrolyte. Decomposition of CO_2 to CO occurs at the cathode. The details are in Eq. (2).

$$\mathrm{CO_2} + 2\mathrm{e^-} \rightarrow \mathrm{CO} + \mathrm{O^{2-}} \tag{2}$$

The generated oxide ions were transferred to the anode through the electrolyte and oxidized to oxygen molecules. The details are in Eq. (3).

$$\mathrm{O^{2-}} \rightarrow 1/2\mathrm{O_2} + 2\mathrm{e^-} \tag{3}$$

As mentioned above, SOECs must be capable of electrolyzing substantial amounts of CO_2 for application in energy systems such as iACRES. Therefore, they require large output and reaction areas. To achieve this, SOECs must have a large cell area. However, very large ceramic-supported SOECs lack mechanical strength. Particularly in anode-supported SOFCs, the nickel–yttria stabilized zirconia (Ni-YSZ) used tends to convert into NiO-YSZ when exposed to oxidative conditions. This can expand the volume of the anode and damage the cells [12]. In light of this, we propose a metal-supported SOEC (MS-SOEC), which is expected to have higher mechanical strength [11,13]. Comparing the flexural strength, stainless steel SUS316L is about 900 MPa, whereas ceramic NiO-YSZ is about 200 MPa [14,15]. In addition, the use of metal instead of ceramics for the support not only improves the mechanical strength but also reduces manufacturing costs [16]. Because of these improvements, we expect the development of large-area cells for MS-SOECs will receive considerable attention.

In a previous study, MS-SOECs developed in our laboratory with an electrolyte thickness of 300 μm could perform CO_2 electrolysis with a current density of 156 mA cm^{-2} at 4 V using the two-terminal method [11]. However, the electrolytic performance of MS-SOECs needs further improvement of both the current density and electrolysis rate. In this study, we evaluated the effects of denser solid electrolytes with smaller electrolyte particle sizes on the electrochemical performance of MS-SOECs.

2. Experimental

2.1. Configuration of metal-supported solid oxide electrolysis cells

In the MS-SOEC, we formed an SOEC structure on a stainless-steel mesh support. We made the support from SUS430, consisting of a 20 mm diameter disk with a mesh layer made from SUS316L (Nippon Seisen, Co., Ltd.). In addition, we designed the metal substrate with seven hexagonally-arranged 3 mm holes to provide stability to the substrates.

The MS-SOEC had a four-layer structure consisting of anode, electrolyte, cathode, and diffusion barrier layer (DBL): $La_{0.6}Sr_{0.4}Co_{0.2}Fe_{0.8}O_{3-\delta}$ (LSCF), YSZ, NiO-YSZ, and $La_{0.6}Sr_{0.2}Ca_{0.2}CrO_3$ (LSCC), respectively. All layers were formed by atmospheric plasma spraying (Tocalo Co., Ltd.). As the sprayed particles, LSCF, NiO-YSZ, and LSCC powders were agglomerated and sintered, and then adjusted to a median diameter of 30 μm by sieving. For the sprayed electrolyte particles, YSZ was fused and crushed, and the powders were adjusted to 29 μm and 18 μm in median diameter by sieving. Cells fabricated using electrolytes with median diameters of 29 μm and 18 μm are named as ASS and ASF cells, respectively, and the electrolyte thickness is added to the end of the cell name. In this study, three types of cells, ASS150, ASF150, and ASF75, were prepared and their electrochemical performance was evaluated. **Figure1 (a), (b)** show a photograph of the developed MS-SOEC, and a schematic of its cross-section is in Figure 1 (c).

Figure 2 shows the cross-sectional SEM images of the ASF150 and ASS150 cells before the experiment. In the ASS150 cell shown in Figure 2 (a), we observed 5–10 μm pores in the YSZ electrolyte layer. In contrast, the number of pores in the YSZ layer of the ASF150 cell was clearly reduced (Figures 2 (b)). Color thresholding image of the electrolyte area in the cross-sectional SEM image of each sample is shown in Figures 2(c) and (d). The horizontal and vertical sizes of the extracted area are 400 and 100 μm. Image analysis [17] of these threshold color images shows that the porosity of the electrolyte of ASS150 and ASF150 is 10.9% and 5.5%, respectively. In the thermal spraying method, the powder is flattened after melting, so the porosity does not always correspond to the sprayed particle size. However, in the MS-SOEC produced in this study, it was confirmed that the change in sprayed particle size from 29 to 18 μm had a significant effect on the electrolyte densification.

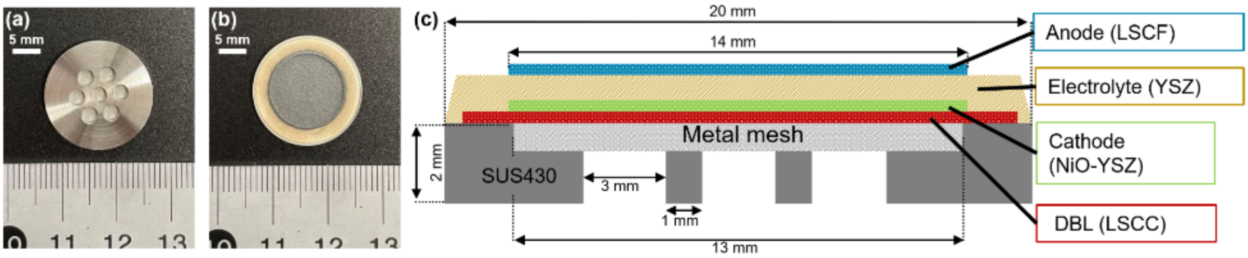

Figure 1. Photograph of ASF150 taken from (a) base metal side, and (b) anode side, and (c) schematic diagram of cross-sectional structure of the cell.

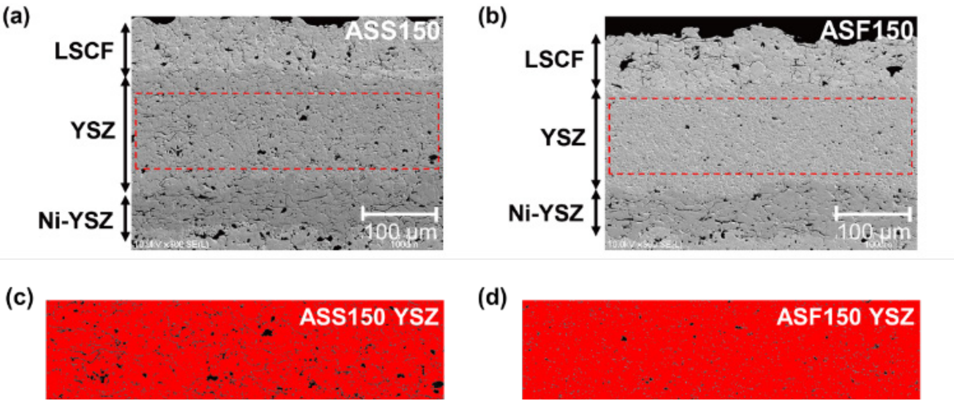

Figure 2. Cross-sectional SEM image of (a) ASS150 and (b) ASF150 prior to experimentation, and threshold color image of (c) ASS150 and (d) ASF150 electrolyte section (400μm x 100μm, area enclosed by dashed lines).

2.2. Characterization of metal-supported solid oxide electrolysis cells

A diagram of the experimental apparatus used to evaluate the performance of MS-SOECs is in **Figure 3 (a)**. In addition, **Figure 3 (b)** shows a cross-sectional schematic of the MS-SOEC. The cell was held in place by two outer alumina tubes with glass-sealing rings, and the reaction gas was supplied from the inner tube. To investigate the performance of MS-SOECs, we conducted a CO_2 decomposition experiment at 800 °C using the two-terminal method. The electrochemical performance of the MS-SOECs was evaluated using a potentiostat/galvanostat (HZ-7000, HOKUTO DENKO Corp.). The impedance of each MS-SOEC was measured at 3 V within the frequency range of 100 kHz to 1 mHz. We measured the current density–voltage curves (I-V curves) in the voltage range 0.25–5.0 V. For further investigation of the cell performance, we conducted gas analyses on both electrode sides using gas chromatography (GC-8A, SHIMADZU Corp.). The ratio of CO_2, H_2, and N_2 fed to the cathode was 10:1:9, and only N_2 gas entered the anode side. The total flow rate was 40 mL min^{-1} for both electrode sides, established with a mass flow controller (MODEL3660, KOFLOC Corp.). We obtained cross-sections of MS-SOECs using a field emission scanning electron microscope (FE-SEM, JSM-7500F, JEOL Ltd.)

3. Results and discussion

3.1. Electrochemical performance evaluation

Figure 4 (a) shows the I-V curves of ASS150, ASF150, and ASF75. The current density increased rapidly from a voltage around 0.8 V, which is attributed to the electrolysis of CO_2. The ASF150 and ASF75 cells with denser electrolytes showed improved performance compared to the ASS150 cell, owing to the use of a finer electrolyte particle size. The current density at 4 V was 195 mA cm^{-2} for the ASF150 cell and 203 mA cm^{-2} for the ASF75 cell compared to 155 mA cm^{-2} for the ASS150 cell. This result suggests that electrolyte densification improved the oxygen ion conductivity. The impedance spectra are in **Figure 4 (b)** and fitting was performed based on the equivalent circuit model shown in **Figure 4 (c)**. The components of resistance obtained from the fitting are shown in **Table 1**. R_s is the ohmic drop; R_h and R_l are the diffusion resistances on the high- and low-frequency sides, respectively; and R_t is the

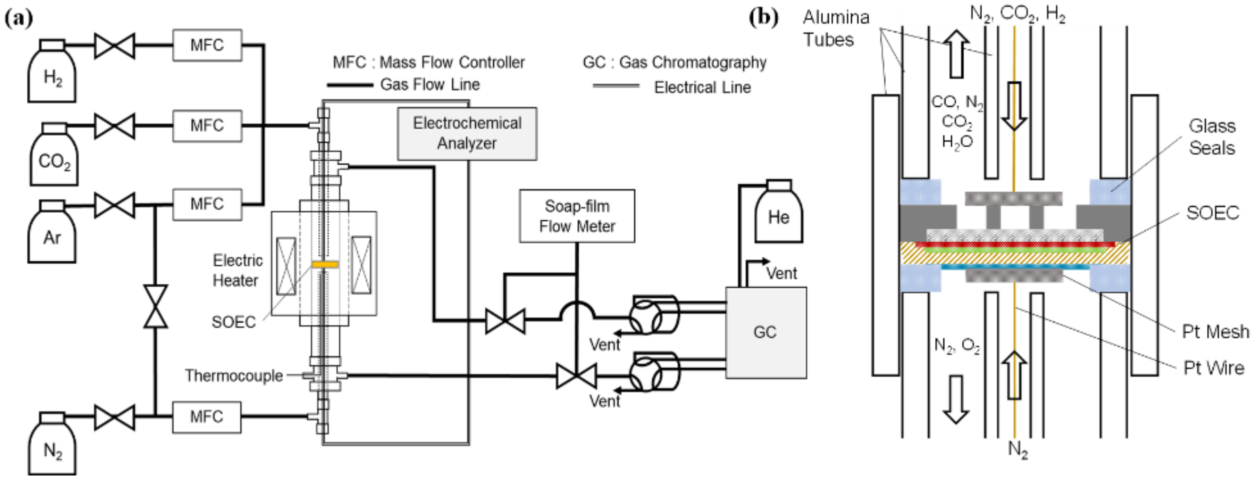

Figure 3. (a) Schematic diagram of the experimental apparatus for CO_2 electrolysis and (b) cross-sectional structure around MS-SOEC.

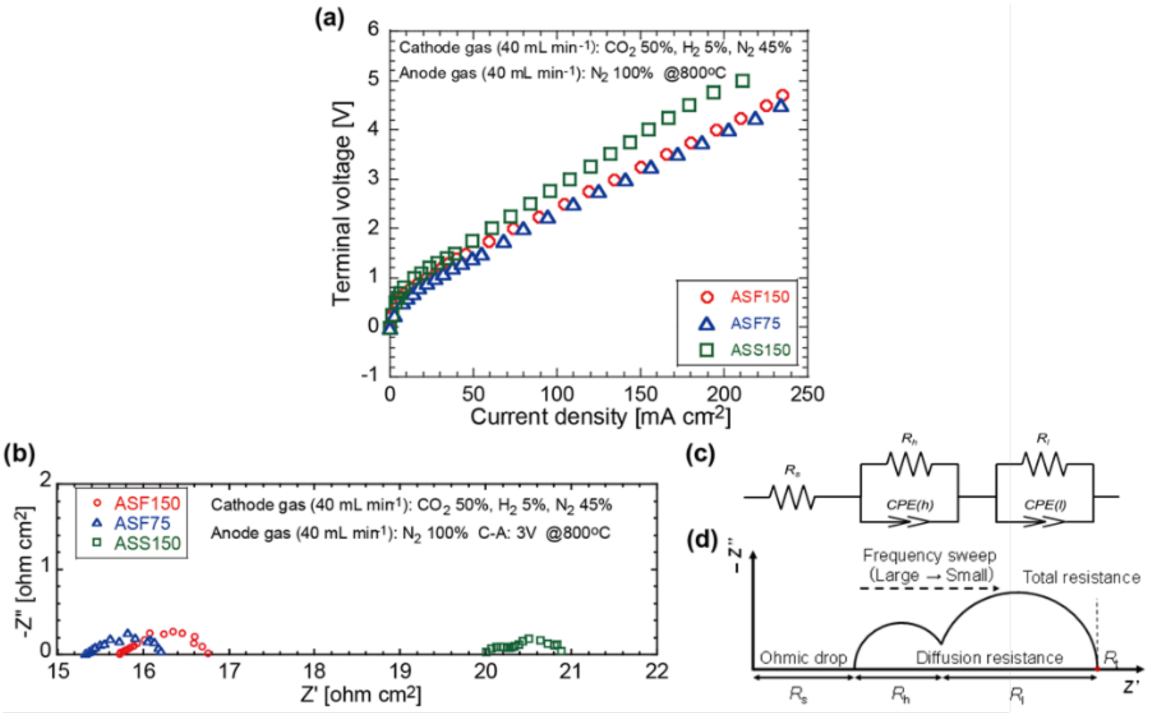

Figure 4. Electrochemical performance of ASS150, ASF150, and ASF75 in CO_2 electrolysis at 800°C.
(a) I-V curve, (b) impedance plots of the cell at 3 V, (c) equivalent circuit, and (d) schematic image of Nyquist plot with explanation of resistances

total resistance (R_s+R_h+R_l). Each of the resistance components obtained from Table 1 corresponds to the Nyquist plot in **Figure 4 (d)**. Figure 4 (b) shows that the ohmic drop (R_s) of electrolyte-densified ASF150 and ASF75 is approximately 15 Ω cm^2. This is lower than the ohmic drop of ASS150, which is approximately 20 Ω cm^2. The ohmic drop of ASF150 and ASF75 was obtained to be 15.7 and 15.3 Ω cm^2, respectively. Since the reported electronic transport per unit thickness of YSZ is 3.1 Ω cm [18], the electronic transport of the electrolyte fabricated by the atmospheric spraying method is about 58% of the reported value. The reported electronic transport of the electrolyte fabricated by the atmospheric plasma spraying method is about 58% of 3.1 Ω cm. The diffusion resistances (R_h + R_l) of ASF150, ASF75, and ASS150 were 1.03, 0.91, and 1.16 Ω cm^2, respectively, which are minor changes compared to the ohmic drop. Therefore, electrolyte densification may have contributed to the decrease in ohmic drop.

Table 1. Resistance values for ASF150, ASF75, and ASS150 obtained from impedance analysis

MS-SOEC	Resistance [Ω cm^2]			
	R_s	R_h	R_l	R_t
ASF150	15.7	0.09	0.94	16.8
ASF75	15.3	0.05	0.86	16.2
ASS150	20.0	0.28	0.88	21.2

3.2. Results of gas analysis

Figure 5 (a)–(c) show the CO and O_2 production rates versus current density for each MS-SOEC. Note that the total CO production rate includes two reactions: CO_2 decomposition by electrolysis and the reverse water-gas shift reaction. We calculated the CO production rate of electrolysis by subtracting the detected water production rate from the total CO production rate. In all cells, the CO and O_2 production rates increased with increasing current density.

To compare the three MS-SOECs, **Figure 5 (d)** shows the CO production rate of each MS-SOEC when we applied equal potentials in the range 2–5 V. At 4 V, the CO production rate of the ASF150 cell was 0.635 μmol s^{-1} cm^{-2}, which was approximately 1.4 times higher than the CO production rate of the ASS150 cell of 0.446 μmol s^{-1} cm^{-2}. We attribute this to the improved electrochemical performance, as confirmed by the I-V curves and impedance measurements. The electrolyte particle size was reduced from d_{50} = 29 μm to d_{50} = 18 μm, which may have contributed to the densification of the electrolyte layer and reduced gas leakage in the cell, thereby suppressing the recombination reaction between CO and O_2. However, the ASF75 cell had a CO production rate of 0.481 μmol s^{-1} cm^{-2} at 4 V, which is inferior to the ASF150 cell. This is due to the thinner electrolyte and increased leakage rate inside the cell. This suggested that, in addition to the leakage of CO_2 to the anode side before electrolysis, the leakage of the generated CO to the anode side contributed to the recombination reaction with O_2. Conversely, the I-V curve shows that the current density at 4 V is approximately 4% higher for ASF75 (203 mA cm^{-2})

than for ASF150 (195 mA cm^{-2}). This contributes to the decrease in the total resistance owing to the decrease in the electrolyte thickness. **Figure 5 (e)** shows the Faraday efficiency of each cell at various current densities. ASF150 shows the highest Faraday efficiency of 80% at a current density of 74 mA cm-2, while both ASF75 and ASS150 show values of about 50-60% at current densities between 50 and 250 mA cm-2. The Faraday efficiency decrease in the MS-SOECs evaluated in this study may have been caused by migration or re-oxidation of the produced CO gas due to cross-leakage of the gases. In particular, the observed decrease in Faraday efficiency at high current densities in the ASF150 may be caused by a higher concentration of the produced gas at the cell surface, resulting in an increase the leakage amount. Based on these results, further densification and thinning of the YSZ layer to improve the CO formation rate and electrochemical performance should be future goals.

4. Conclusion

In this study, we evaluate a metal-supported solid oxide electrolysis cell as a carbon dioxide reduction process for the realization of iACRES. To develop MS-SOECs for more efficient CO_2 electrolysis, the electrolyte particle size was changed from d_{50} = 29 μm to d_{50} = 18 μm to increase electrolyte density. Cross-sectional observation by SEM confirmed that the 5–10 μm pores observed in the electrolyte layer of ASS150 were reduced in number and became denser. Regarding the performance of ASF150, a current density of 195 mA cm^{-2} at 4 V and CO production rate of 0.635 μmol s^{-1} cm^{-2} were obtained. Compared to ASS150 without electrolyte densification, the current density and CO production rate were approximately 1.3 and 1.4 times higher, respectively. The ASF75 cell with a thinner electrolyte exhibited an increased gas leakage rate inside the cell, resulting in a reduced CO production rate (0.481 μmol s^{-1} cm^{-2} at 4 V). However, the current density of ASF75 was 205 mA cm^{-2} at 4 V, which was 4% higher

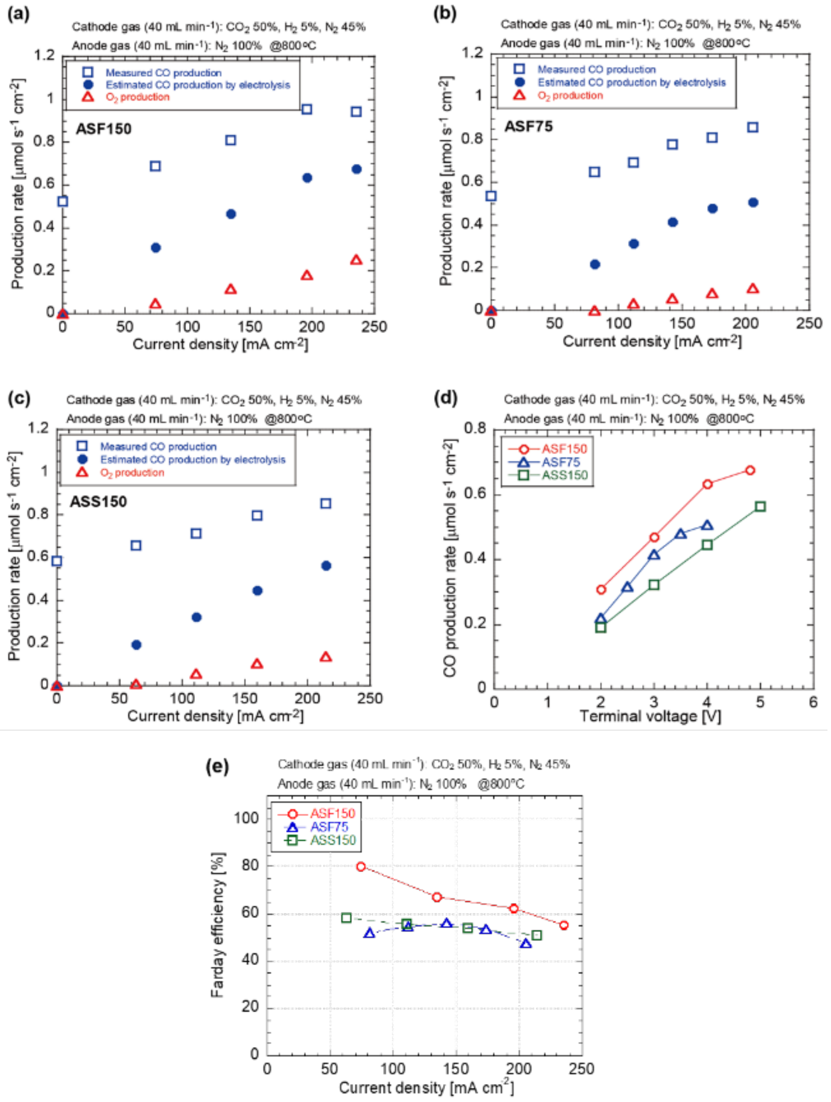

Figure 5. CO and O_2 production rate for (a) ASF150, (b) ASF75 and (c) ASS150 in cathode and anode side, (d) CO production by electrolysis as a function of applied voltage, and (e) Faraday efficiency under each current density in CO_2 electrolysis at 800°C.

than that of ASF150. Therefore, increased densification and thinning of the electrolyte should be investigated to further improve the CO_2 electrolysis performance of MS-SOEC.

Acknowledgements

This research was based on results obtained from a project, JPNP16002, commissioned by the New Energy and Industrial Technology Development Organization (NEDO). This research was also supported by JSPS KAKENHI Grant Number JP19H02807. The authors also thank Materials Analysis Division, Open Facility Center, Tokyo Institute of Technology, for SEM observation.

References

[1] K. Hashimoto, Global Temperature and Atmospheric Carbon Dioxide Concentration (2019), pp. 5-17.

[2] L.L. Simon, The Paris Agreement has solved a troubling problem, *Nature* 532 (2016), p. 283.

[3] K.K. Kurramovich, A.A. Abro, A.I. Vaseer, S.U. Khan, S.R. Ali and M. Murshed, Roadmap for carbon neutrality: the mediating role of clean energy development-related investments. *Environ. Sci. Pollut. Res.* 29 (2022), pp. 34055-34074.

[4] Y. Kato, Carbon Recycling for Reduction of Carbon Dioxide Emission from Iron-making Process, *ISIJ Int*. 50 (2010), pp. 181-185.

[5] Ministry of the Environment, *National Greenhouse Gas Inventory Report of JAPAN* (2012).

[6] S. Michitaka, Y. Tetsuya and S.Masaaki, Recent Progress in Ironmaking Technology for CO_2 Mitigation at JFE Steel. *JFE Tech. Rep*. 19 (2014), pp. 103-109.

[7] Y. Kato, Utilization of HTGR on active carbon recycling energy system. *Nucl. Eng. Des*. 271 (2014), pp. 79-83.

[8] S.D. Ebbesen and M. Mogensen, Electrolysis of carbon dioxide in Solid Oxide Electrolysis Cells, *J. Power Sources* 193 (2009), pp. 349-358.

[9] S. Lee, M. Kim, K.T. Lee, J.T.S. Irvine and T.H. Shin, Enhancing Electrochemical CO_2 Reduction using $Ce(Mn,Fe)O_2$ with $La(Sr)Cr(Mn)O_3$ Cathode for High-Temperature Solid Oxide Electrolysis Cells, *Adv. Energy Mater.* 11 (2021).

[10] L. Ye, C. Pan, M. Zhang, C. Li, F. Chen, L. Gan and K. Xie, Highly Efficient CO_2 Electrolysis on Cathodes with Exsolved Alkaline Earth Oxide Nanostructures, *ACS Appl. Mater. Interfaces* 9 (2017), pp. 25350-25357.

[11] H. Takasu, Y. Maruyama and Y. Kato, Development of metal supported SOEC for carbon recycling iron making system, ISIJ Int. 60 (2020), pp. 2870-2875.

[12] M.C. Tucker, Durability of symmetric-structured metal-supported solid oxide fuel cells, *J. Power Sources* 369 (2017), pp. 6-12.

[13] Y. Numata, K. Nakajima, H. Takasu and Y. Kato, Carbon dioxide reduction on a metal-supported solid oxide electrolysis cell, *ISIJ Int.* 59 (2019), pp. 628-633.

[14] C.R. He and W.G. Wang, Alumina doped Ni/YSZ anodematerials for solid oxide fuel cells, *Fuel Cells* 9 (2009), pp. 630-635.

[15] A. Kasha, S.O. Obadimu and K.I. Kourousis, Flexural characteristics of material extrusion steel 316L: Influence of manufacturing parameters, *Addit. Manuf. Lett*. 3 (2022), 100087.

[16] M.C. Tucker, Progress in metal-supported solid oxide fuel cells: A review, *J. Power Sources* 195 (2010), pp. 4570-4582.

[17] C.A. Schneider, W.S. Rasband and K.W.Eliceiri, NIH Image to ImageJ: 25 years of image analysis, *Nature Methods*, 9 (2012), pp. 671-675.

[18] J. Park and R.N. Blumenthal, Electronic Transport in 8 Mole Percent Y2O3-ZrO2, *J. Electrochem. Soc.* 136 (1989), p. 2867.